Quantifying nitrous oxide emissions in the U.S. Midwest - A top-down study using high resolution airborne in situ observations

Maximilian Eckl[1], Anke Roiger[2], Julian Kostinek[2], Alina Fiehn[2], Heidi Huntrieser[2], Christoph Knote[3], Zachary Robert Barkley[4], Stephen Ogle[5], Bianca C. Baier[6], Colm Sweeney[7], and Kenneth J. Davis[4]

[1]Deutsches Zentrum für Luft- un Raumfahrt
[2]Deutsches Zentrum für Luft- und Raumfahrt
[3]Ludwig-Maximilians-University
[4]Pennsylvania State University
[5]Colorado State University
[6]University of Colorado Boulder
[7]NOAA Global Monitoring Laboratory

November 21, 2022

Abstract

The U.S. Midwest, with its intensive agriculture, is a prominent source of nitrous oxide (N2O) but top-down and bottom-up N2O emission estimates differ significantly. We quantify Midwest N2O emissions by combining observations from the Atmospheric Carbon and Transport-America campaign with model simulations to scale the Emissions Database for Global Atmospheric Research (EDGAR). In October 2017 we increased agricultural EDGAR version 4.3.2/5.0 emissions by a factor of 6.3±4.6/3.5±2.7, resulting in Midwest N2O emissions of 0.42±0.28 nmol m-2 s-1. In June/July 2019, a period when extreme flooding was occurring in the Midwest, EDGAR was increased by a factor of 11.4±6.6/9.9±5.7, resulting in N2O emissions of 1.06±0.57 nmol m-2 s-1. Agricultural emissions estimated with the process-based model DayCent (Daily version of the CENTURY ecosystem model) were larger than in EDGAR but still substantially smaller than our estimates. Due to the complexity of N2O emissions, further studies are necessary to fully characterize Midwest emissions.

Quantifying nitrous oxide emissions in the U.S. Midwest - A top-down study using high resolution airborne in situ observations

Maximilian Eckl[1], Anke Roiger[1], Julian Kostinek[1], Alina Fiehn[1], Heidi Huntrieser[1], Christoph Knote[2], Zachary R. Barkley[3], Stephen M. Ogle[4], Bianca C. Baier [5,6], Colm Sweeney[6], and Kenneth J. Davis[3,7]

[1]Deutsches Zentrum für Luft- und Raumfahrt (DLR), Institut für Physik der Atmosphäre, Oberpfaffenhofen, Germany
[2]Ludwig-Maximilians-University (LMU), Meteorological Institute, Munich, Germany
[3]Department of Meteorology and Atmospheric Science, Pennsylvania State University, University Park, PA, USA
[4]Natural Resource Ecology Laboratory, Colorado State University, Fort Collins, CO, USA
[5]Cooperative Institute for Research in Environmental Sciences, University of Colorado-Boulder, Boulder, CO, USA
[6]NOAA Global Monitoring Laboratory, Boulder, CO, USA
[7]Earth and Environmental Systems Institute, Pennsylvania State University, University Park, PA, USA

Key Points:

- Within the ACT-America project we gathered a unique airborne in situ N_2O data set over the U.S. Midwest with enhancements up to 9 ppb
- N_2O emissions in the U.S. Midwest were on average $0.42 \pm 0.28\,\mathrm{nmol\,m^{-2}\,s^{-1}}$ in Oct 2017 and $1.06 \pm 0.57\,\mathrm{nmol\,m^{-2}\,s^{-1}}$ in Jun-Jul 2019
- Bottom-up estimates from EDGAR and the often four times higher DayCent underestimate U.S. Midwest N_2O emissions by factors up to 20

Corresponding author: Maximilian Eckl, `Maximilian.Eckl@dlr.de`

Abstract

The U.S. Midwest, with its intensive agriculture, is a prominent source of nitrous oxide (N_2O) but top-down and bottom-up N_2O emission estimates differ significantly. We quantify Midwest N_2O emissions by combining observations from the Atmospheric Carbon and Transport-America campaign with model simulations to scale the Emissions Database for Global Atmospheric Research (EDGAR). In October 2017 we increased agricultural EDGAR version 4.3.2/5.0 emissions by a factor of 6.3±4.6/3.5±2.7, resulting in Midwest N_2O emissions of $0.42\pm0.28\,\mathrm{nmol\,m^{-2}\,s^{-1}}$. In June/July 2019, a period when extreme flooding was occurring in the Midwest, EDGAR was increased by a factor of 11.4±6.6/9.9±5.7, resulting in N_2O emissions of $1.06\pm0.57\,\mathrm{nmol\,m^{-2}\,s^{-1}}$. Agricultural emissions estimated with the process-based model DayCent (Daily version of the CENTURY ecosystem model) were larger than in EDGAR but still substantially smaller than our estimates. Due to the complexity of N_2O emissions, further studies are necessary to fully characterize Midwest emissions.

Plain Language Summary

Nitrous oxide (N_2O) is the third most important anthropogenic greenhouse gas contributing to the warming of the planet and the dominant man-made ozone-depleting substance in the stratosphere. Its atmospheric concentrations have been rising since industrialization mainly due to an increase in anthropogenic sources, with agriculture being the dominant source. The densely farmed U.S. Midwest plays an important role in the global N_2O budget. However, previous studies that have collected observations of N_2O indicate that estimates of surface emissions in the Midwest are substantially underestimating the truth. In this study we combine unique aircraft-based N_2O measurements and model simulations to quantify Midwest emissions in October 2017 and June/July 2019. Agricultural inventory estimates had to be increased by factors up to 20 to match observations, revealing a large underestimation in current inventories. An extreme flooding event in 2019 when the summer observations occurred may be responsible for some of this discrepancy. Estimations of soil N_2O emissions calculated with a state-of-the-art biogeochemical model show less underestimation but are still too low compared to the fluxes derived from the aircraft observational data.

1 Introduction

Nitrous Oxide (N_2O) is the third most important anthropogenic greenhouse gas (GHG) in terms of long-term radiative forcing (Myhre et al., 2013) and is the dominant ozone depleting substance in the stratosphere (Ravishankara et al., 2009). Global N_2O concentrations are 333 ppb as of April 2020, approximately a 20 % increase since preindustrial times (MacFarling Meure et al., 2006; NOAA-ESRL, 2020). Anthropogenic sources like agriculture and fossil fuel combustion contribute to this trend (Ciais et al., 2013). In recent years, those N_2O emissions have increased at a higher rate than expected (Thompson et al., 2019; Tian et al., 2020). Agricultural soil management associated with reactive forms of nitrogen (N) (i.e. mineral fertilizer, livestock manure additions, and legumes) accounts for half of global N_2O emissions (Paustian et al., 2016). Analyses of the isotopic composition of N_2O indicate that the observed rise in global atmospheric N_2O concentrations is mainly caused by the increased application of N-fertilizers (Park et al., 2012).

Bottom-up estimates, such as the Emissions Database for Global Atmospheric Research (EDGAR, 2020), use emission factors and activity data to calculate emissions. However, the nature of N_2O soil emissions complicates their quantification. Agricultural practices (e.g. fertilizer application rate, crop type) as well as meteorological and soil conditions (e.g. precipitation, soil moisture) directly influence emissions, resulting in large temporal variability in N_2O surface fluxes (Stehfest & Bouwman, 2006). Process-based biogeochemical models like DayCent (Daily version of the CENTURY ecosystem model) provide a more sophisticated approach for estimation of N_2O emission by simulating soil processes based on various environmental drivers. Nevertheless, fluxes at regional scale are still highly uncertain due to insufficient direct observations (Reay et al., 2012).

The U.S. Midwest is one of the most intensively cultivated agricultural regions worldwide (FAO, 2020; USDA-NASS, 2020), thus contributing significantly to the global anthropogenic N_2O emissions (Miller et al., 2012). Previous top-down studies indicate that emissions in the Midwest are underestimated by EDGAR, but are highly uncertain on the magnitude of this underestimation (Kort et al., 2008; Miller et al., 2012; Griffis et al., 2013; Chen et al., 2016; Fu et al., 2017). Kort et al. (2008) showed that EDGAR version 32FT2000 underestimates emissions in May-June 2003 by a factor of 2.62 over the central U.S. and southern Canada. Miller et al. (2012) derived scaling factors of 6.1 and 10.1 for EDGAR version 4 for June 2004 and June 2008, respectively. Fu et al. (2017) concluded even higher scaling factors for agricultural EDGAR version 4.2 emissions in the Corn Belt region of the Midwest, with scaling factors of 19.0-28.1 in June 2010. These described top-down studies used tall tower measurements, characterized by long time series over several months but limited in their spatial coverage. Only Kort et al. (2008) used aircraft-based flask measurements, which provide some spatial (central U.S. and southern Canada) but limited temporal (May-June 2003) coverage. The large range in the quantitative results show that Midwest N_2O surface fluxes are underestimated by EDGAR inventories, but their true values are highly uncertain.

In this study we quantify N_2O emissions for several flights conducted in parts of the U.S. Midwest in October 2017 and June/July 2019 with a top-down approach. Unlike previous studies which have relied on observations with limited spatial coverage, this study uses continuous airborne in situ measurements of N_2O. By combining these observations with forward model simulations, we optimize agricultural fluxes from EDGAR version 4.3.2 and version 5.0 to quantify Midwest N_2O emissions. The employed method was already successfully applied in several methane top-down studies (Barkley et al., 2017; Barkley, Davis, et al., 2019; Barkley, Lauvaux, et al., 2019). The derived emission rates are finally compared to flux estimates of direct soil emissions produced with EDGAR and the biogeochemical model DayCent (Parton et al., 1998; Del Grosso et al., 2001, 2011).

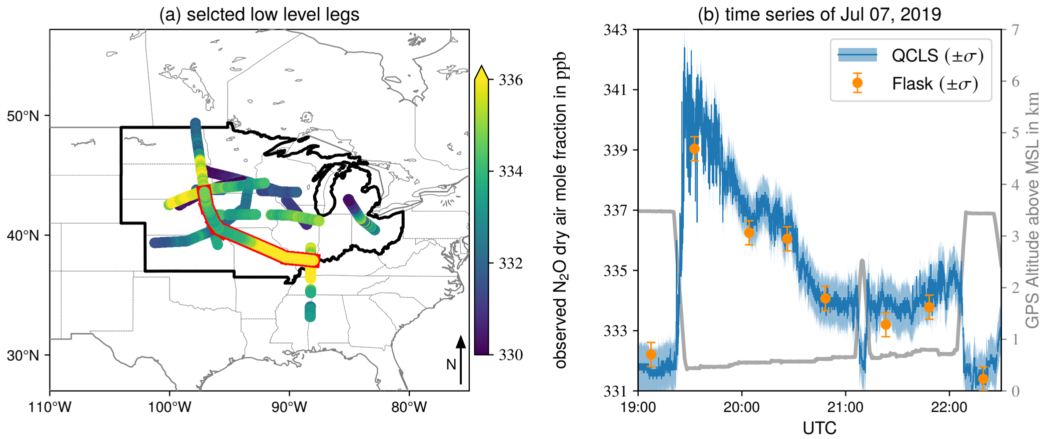

Figure 1. (a) Selected low level legs (at approx. 1000 ft AGL) of the ACT-America campaigns in 2017 and 2019, color-coded with observed N_2O dry air mole fractions. The study region (Midwest) is encircled by a thick black line. (b) Time series of N_2O dry air mole fraction of the flight on July 07, 2019 with error bars indicating ± 0.8 ppb and coincident NOAA/GML flask measurements of N_2O (± 0.4 ppb). The corresponding transect in (a) is encircled in red.

2 Data and Methods

2.1 Observational Data

We use measurements from the Atmospheric Carbon and Transport-America (ACT-America, `https://act-america.larc.nasa.gov/`) campaign. ACT-America includes five airborne campaigns from 2016 to 2019, providing a rich data set of in situ and remote greenhouse gas measurements in all four seasons. During the fall 2017 (10 Oct - 13 Nov) and summer 2019 (17 Jun - 27 Jul) field deployments, we collected approximately 60 h of in situ data onboard NASA's C-130 with an Aerodyne Quantum Cascade Laser Spectrometer (QCLS) measuring N_2O mole fractions (among others) at 2 Hz with an uncertainty of 0.8 ppb (Kostinek et al., 2019). Every 3-10 minutes in-flight calibrations were performed using standards that were cross-calibrated after the campaign against NOAA/GML standards traceable to the NOAA-2006A scale (Hall et al., 2007). Additionally, during each flight 6-12 whole-air flask samples were taken by NOAA/GML and measured for trace gases including N_2O with an uncertainty of 0.4 ppb (Sweeney et al., 2015, 2018; Baier et al., 2020). Those were merged into the QCLS time series to fill any data gaps.

For this study we selected four flights from 2017 (October) and six flights from 2019 (June/July). For each flight the C-130 flew low level legs well within the planetary boundary layer (PBL) ($\sim$1000 ft above ground level (AGL)) for at least 45 min during which Midwest air was sampled. Figure 1a shows the selected transects, color-coded with observed N_2O dry air mole fractions. These flights cover most parts of the Midwest. Mole fractions up to 341 ppb were observed (Figure 1b). We are not aware of comparable continuous N_2O measurements spanning most of Midwest across two seasons, highlighting the unique opportunity to quantify Midwest emissions with these data.

2.2 Model Setup

The Weather Research and Forecasting model with chemistry enabled version 4.0.2 (WRF-Chem; Grell et al. (2005)) is used to propagate N_2O enhancements emitted from emission inventories (Section 2.3) throughout the atmosphere. Initial N_2O concentrations and the inflow at the boundaries of the model domain are set to zero. Thus, we simulate only enhancements caused by emissions within the model domain. We treat N_2O as a passive tracer due to its long atmospheric lifetime of ~ 116 years (Prather et al., 2015). The model domain consists of an outer and inner domain with a horizontal resolution of 15 km × 15 km and 3 km × 3 km, respectively. The outer domain, centered over the Midwest, covers nearly the whole continental U.S., northern Mexico, and southern Canada (Figure 2a), whereas the extension and position of the inner domain is separately chosen for each flight so that the low level legs are spaciously encapsulated. We perform each simulation with three different meteorological initial and boundary conditions: The 5^{th} generation atmospheric reanalysis data (ERA5, 2017; Hersbach et al., 2020), the North American Regional Reanalysis (NARR, 2005), and the Global Data Assimilation System Final analysis (GDAS-FNL, 2015). As in Barkley, Davis, et al. (2019), we use these different simulations to estimate model transport errors (Díaz-Isaac et al., 2018). See the supporting information (SI) for additional information about the model setup.

2.3 Emission Inventories

The prior N_2O surface emission estimates for the optimization were obtained from EDGAR version 4.3.2 (EDGAR4.3.2, 2017; Janssens-Maenhout et al., 2019) and version 5.0 (EDGAR5.0, 2019; Crippa et al., 2020). For this study the different sectors in the inventories were merged into three main sectors: agricultural E_{AGR}, anthropogenic non-agricultural E_{nonAGR}, and natural emissions E_N (see SI). We assume that these three sectors cover all N_2O emissions in the model domain. EDGAR4.3.2 and EDGAR5.0 provide monthly resolved N_2O fluxes from anthropogenic source (E_{AGR} and E_{nonAGR}) on a $0.1^\circ \times 0.1^\circ$ grid for 2012 and 2015, respectively, but do not include fluxes from natural sources. Hence, we supplemented both versions with yearly E_N on a $1^\circ \times 1^\circ$ grid from EDGAR version 2.0 (EDGAR2; Olivier et al. (1996, 1999)). All fluxes are assumed to originate from the surface.

With the process-based, biogeochemical model DayCent we estimated daily direct N_2O soil emissions from crop- and grassland on a $0.5^\circ \times 0.5^\circ$ grid in the Midwest from 2011 to 2015, which were aggregated to a monthly time step. The model simulates fluxes of carbon and nitrogen between the atmosphere, vegetation, and soil thus deriving N_2O emissions. Incorporating several environmental drivers, including weather patterns, agricultural practices, soil characteristics, and crop features, this approach provides a more sophisticated estimate of soil emissions than the emission factor based EDGAR inventory. The GHG inventory of the United States Environmental Protection Agency (EPA, 2020) uses DayCent estimates of direct soil emissions for emissions reporting of agricultural soil N_2O to the UN Framework Convention on Climate Change. DayCent does not calculate emissions from manure management, agricultural waste burning, indirect soil emissions, and those associated with minor crops such as vegetables. The EPA inventory quantifies these sources and subsources with an emission factor approach. We estimate their contribution by employing the yearly estimates from EPA, calculating their relative fraction of the EPA direct soil emissions, and adding them to our monthly estimates. As a result, our DayCent inventory properly accounts for the total agricultural emissions, but not the spatial distribution of agricultural sources which are not estimated by DayCent.

2.4 Optimization Technique

To solve for N_2O emissions, we use an approach similar to the optimization described in Barkley et al. (2017). First, we calculate the observed N_2O enhancements by subtracting a background from the measured absolute mole fraction. For each campaign we derive one background by taking the 2^{nd} percentile of all low level legs of the entire campaign (see SI). The background is defined campaign-wise rather than transect-wise because during some transects we were not able to measure background mole fractions as we started a low level leg within a plume and did not exit the plume inside of the PBL (Figure 1b).

With observed N_2O enhancements calculated, we then compare modeled N_2O enhancements emitted from our prior emission estimate ($E_{AGR}+E_{nonAGR}+E_N$) to the observed enhancements. Differences between model and observed enhancements are then minimized for each flight by scaling agricultural emissions E_{AGR} with a factor F_{AGR} thus quantifying emissions. This process is reliant on the assumption that the discrepancy between the observed and modeled N_2O is driven primarily by errors in the E_{AGR}. As agricultural emissions are the dominant N_2O source in our flights, we scale E_{AGR}, assuming that errors in E_{nonAGR} and E_N are inconsequential to the overall solution. The complexity of N_2O soil emissions suggests that E_{AGR} exhibits a much higher uncertainty than other sources (Butterbach-Bahl et al., 2013), supporting the presented approach.

As an equation, this optimization technique is described by calculating F_{AGR} through the minimization of the following cost function:

$$J(F_{AGR}) = |A_{obs} - \underbrace{(F_{AGR} \cdot A_{AGR} + A_{nonAGR} + A_N)}_{=A_{mod}(F_{AGR})}| \tag{1}$$

A_{obs} and A_{mod} are the time integral along a transect of observed and modeled enhancements, respectively (e.g., area below plume in Figure 3a). A_{mod} consists of an agricultural portion A_{AGR} scaleable with F_{AGR}, a non-agricultural anthropogenic portion A_{nonAGR}, and a natural portion A_N. We compare integrals rather than enhancements themselves because we are interested in the amount of N_2O emitted in the atmosphere. Neither the model transport nor the inventory is perfect and even small uncertainties in just one of them could cause a shift or deformation in the alignment of the modeled plume relative to the observed plume. By minimizing the difference in the total N_2O enhancements rather than the point-by-point absolute error, we preserve the capability to solve for total N_2O emissions even when the modeled and observed plumes do not align. Due to the linearity between A_{AGR} and the area averaged E_{AGR} (see SI), a F_{AGR} derived with equation 1 denotes a F_{AGR}-folded E_{AGR}.

2.5 Uncertainty Assessment

We adopted the method of Barkley, Davis, et al. (2019) to assess uncertainties in our solutions. F_{AGR} is affected by uncertainties in the following variables:

1. observed background mole fraction
2. A_{nonAGR}
3. A_N
4. model transport
5. model wind speed and PBL height
6. spatial distribution in EDGAR emissions

We quantify the influence of uncertainties 1 to 4 by using a Monte Carlo approach. For each flight we repeat the optimization 10 000 times with a perturbed background mole fraction, A_{nonAGR}, and A_N. For the background we take the value derived from the observations and add a normal random number with $\mu = 0$ ppb and $\sigma = \pm 0.5$ ppb for 2017 and $\sigma = \pm 0.9$ ppb for 2019. A_{nonAGR} and A_N are independently multiplied by a factor drawn from a normal distribution with $\mu = 1.0$ and $\sigma = \pm 0.21$ and $\sigma = \pm 0.42$, respectively. To account for the model transport error, we randomly select one of the three model runs with different meteorological initial and boundary conditions, creating variability in the plume shape. The resulting spread in F_{AGR} is used as its uncertainty. Explanations of the values that represent the uncertainties are in the SI.

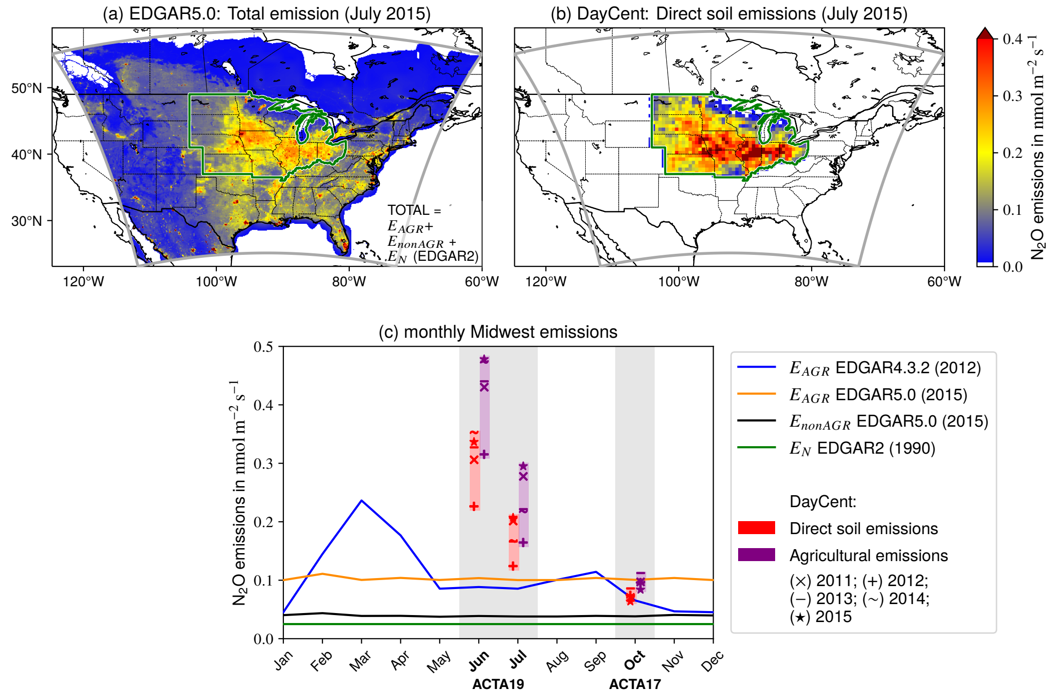

Figure 2. (a) EDGAR5.0 N_2O emissions (plus EDGAR2 E_N) within the model domain (gray box). The Midwest is encircled in green. (b) Direct soil emissions in July 2015 estimated with DayCent. (c) Monthly Midwest emissions. E_{nonAGR} in EDGAR4.3.2 is almost identical to EDGAR5.0. Total agricultural DayCent emissions are estimated utilizing the EPA GHG inventory (Section 2.3).

The modeled wind speed and PBL height uncertainty (source 5), cannot be covered by the Monte Carlo simulation. Errors in these variables cause lower or higher simulated enhancements thus producing biases. Following Barkley et al. (2017) we correct for those biases by applying a correction factor based on the differences between the modeled and observed wind speed and PBL height. On average the modeled wind speed and PBL height is 8 % and 3 % higher than observations, respectively. The impact of this correction on our results is insignificant. Results and further explanations can be found in the SI.

Our final source of uncertainty relates to uncertainties regarding errors in the spatial distribution of the fluxes in the prior inventory, and is difficult to quantify. However, the mapping of emissions in EDGAR is based on several high-resolution proxy data sets (Janssens-Maenhout et al., 2019). For this reason, we assume its spatial errors to be small. Given the insignificant difference between modeled and observed wind speeds and PBL heights, the good agreement between modeled and measured plume structures support this assumption (see SI). Furthermore, because we quantify large area sources and not point sources, slight misplacement in the inventory would only marginally affect our results. At the same time, missing or strongly misplaced fluxes would produce errors that are not considered in this study.

3 Results and Discussion

3.1 Emission Inventory Comparison

Figure 2a shows prior July N_2O emissions in the outermost model domain from anthropogenic EDGAR5.0 and natural EDGAR2 sources. Compared to EDGAR4.3.2 no significant differences in the spatial distribution of emissions is seen, both versions just differ in the strength of the surface fluxes. The largest surface fluxes are concentrated in the Midwest, coinciding with the Corn Belt and its dominant agricultural emissions. Figure 2b shows DayCent direct soil emissions in July 2015. Similar to EDGAR emission maps, the Corn Belt within the Midwest is a prominent source of N_2O. We are not able to perform a detailed comparison of the spatial distributions in EDGAR and DayCent as both do not cover the same set of sources. However, in terms of the overall magnitude, DayCent estimates much higher surface fluxes compared to EDGAR, despite containing fewer sources (gridded total agricultural DayCent emissions are not available; Section 2.3).

Figure 2c displays the monthly evolution of E_{AGR}, E_{nonAGR}, and E_N averaged over the Midwest. Both EDGAR versions have an annual average E_{AGR} of approximately $0.10\,\mathrm{nmol\,m^{-2}\,s^{-1}}$. However, unlike EDGAR5.0, EDGAR4.3.2 exhibits a strong seasonal cycle ranging from $0.05\,\mathrm{nmol\,m^{-2}\,s^{-1}}$ in winter up to $0.24\,\mathrm{nmol\,m^{-2}\,s^{-1}}$ in spring. In spring, when most N-fertilizer is applied, the amount peaks, followed by a plateau during summer at $0.09\,\mathrm{nmol\,m^{-2}\,s^{-1}}$. The harvest season in fall features a local peak at $0.11\,\mathrm{nmol\,m^{-2}\,s^{-1}}$. In a future EDGAR5.0 release a seasonal cycle for some crop related emissions will be implemented (Crippa et al., 2020). E_{nonAGR} shows no significant change over the year and is on average $0.04\,\mathrm{nmol\,m^{-2}\,s^{-1}}$ in both versions. Natural soil emissions account for $0.02\,\mathrm{nmol\,m^{-2}\,s^{-1}}$ per month.

From 2011 to 2015 DayCent emissions in the Midwest range between 0.23–$0.35\,\mathrm{nmol\,m^{-2}\,s^{-1}}$, 0.12–$0.21\,\mathrm{nmol\,m^{-2}\,s^{-1}}$, and 0.06–$0.08\,\mathrm{nmol\,m^{-2}\,s^{-1}}$ in June, July, and October respectively. June and July DayCent emissions are significantly larger than in EDGAR, despite manure management, indirect soil, and agricultural waste burning emissions not being included. DayCent's October emissions are within the magnitude of agricultural EDGAR emissions. We estimate total agricultural Midwest emissions from 2011 to 2015 by combining DayCent direct soil emissions and the EPA GHG inventory (Section 2.3), resulting in 0.32–$0.48\,\mathrm{nmol\,m^{-2}\,s^{-1}}$, 0.16–$0.30\,\mathrm{nmol\,m^{-2}\,s^{-1}}$, and 0.08–$0.11\,\mathrm{nmol\,m^{-2}\,s^{-1}}$ in June, July, and October, respectively. In June/July this is on average over four/two times higher than EDGAR E_{AGR} estimates. The 2012 emissions are significantly lower than in the other years causing the large range across years in the summer months. During this year, the most extensive drought since the 1930s occurred across a large swath of the U.S., including most of the Midwest, which lead to widespread harvest failure (NOAA-NCEI, 2020). This event might explain the low values and indicates that during an average climatological year DayCent emissions are at the upper end of the range. Furthermore, in contrast to EDGAR4.3.2 which states constant emissions in June and July, DayCent emissions are much higher in June than in July. This is consistent with the N_2O climatology in Sweeney et al. (2015).

3.2 Model Optimization

Here, we provide an example of the model optimization process for Oct 10, 2017 (Figure 3a). In the eastern part of the Midwest N_2O enhancements up to 7 ppb were observed within the PBL. The slightly negative values at the beginning of the time series occurred prior to the low level leg in the free troposphere. Our background is derived from air within the PBL and is representative for the time and location of the campaign. Free tropospheric air might have a different history and hence different background which can lead to negative values if we subtract our background. Model simulations with unmodified EDGAR emissions show only enhancements up to 1 ppb along the transect. How-

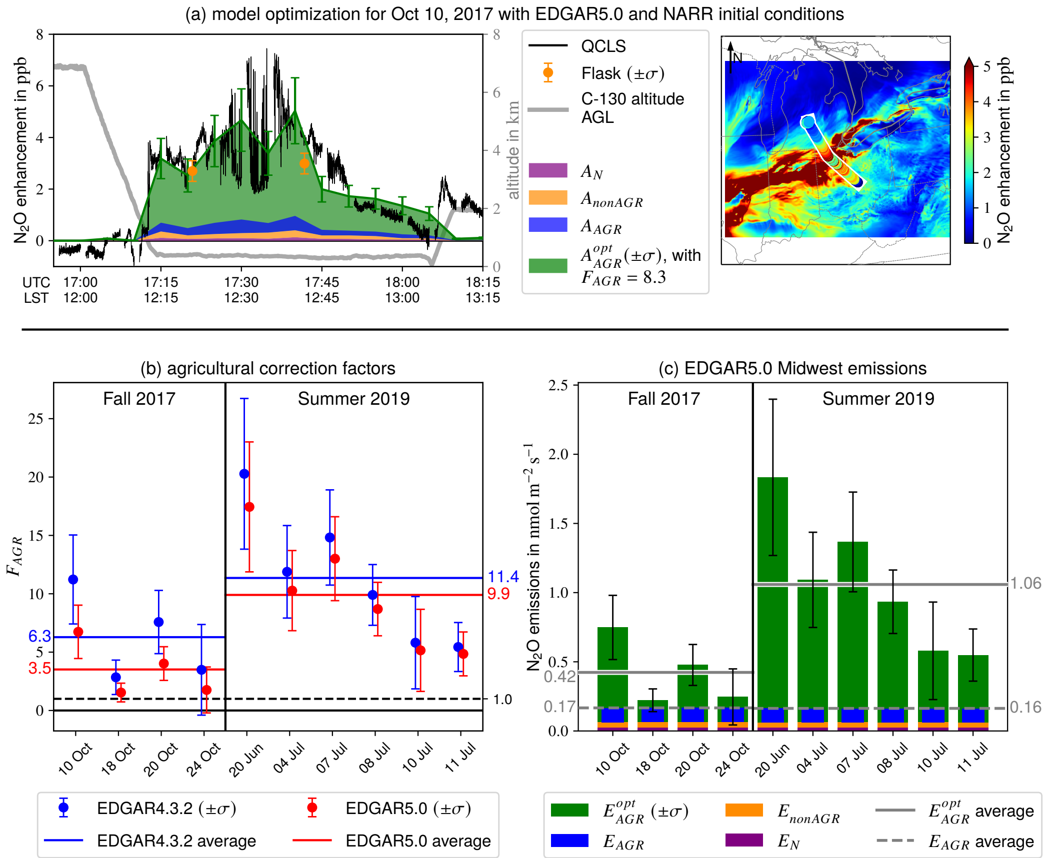

Figure 3. (a) Sample model optimization for Oct 10, 2017 with EDGAR5.0 (plus EDGAR2 E_N) and NARR initial conditions. The left panel shows the prior and optimized modeled N_2O enhancements along the flight track together with observed enhancements. The right panel shows a map of optimized modeled N_2O enhancements (from $E^{opt}_{AGR} + E_{nonAGR} + E_N$) at 300 m AGL at 17:30 UTC and the flight track color-coded with the observed enhancements. (b) Mean and standard deviation of agricultural correction factors F_{AGR} for the investigated research flights resulting from Monte Carlo simulations. (c) EDGAR5.0 Midwest N_2O emissions with optimized and prior E_{AGR}.

ever, by applying an agricultural correction factor F_{AGR} of 8.3 the model is able to reproduce our measurements. Optimizations of the remaining days can be found in the SI.

Figure 3b shows the mean and standard deviation for F_{AGR} of the Monte Carlo simulations of the ten research flights for the two EDGAR versions. As both inventories have a comparable spatial distribution, factors vary due to differences in total emissions. EDGAR4.3.2 correction factors are considerably higher for October 2017 and slightly higher for June/July 2019 than EDGAR5.0. For EDGAR4.3.2, F_{AGR} ranges from 2.9 ± 1.5 to 11.3 ± 3.8 in 2017, with an average factor of 6.3 ± 4.6. EDGAR5.0 F_{AGR} is calculated to be lower but still ranges from 1.6 ± 0.8 to 6.8 ± 2.3, with an average factor of 3.5 ± 2.7. For 2019 we modified EDGAR4.3.2 with a F_{AGR} between 5.5 ± 2.1 and 20.2 ± 6.3 and EDGAR5.0 between 4.9 ± 1.9 and 17.4 ± 5.5. On average this denotes an agricultural correction factor of 11.4 ± 6.6 and 9.9 ± 5.7 for EDGAR4.3.2 and EDGAR5.0, respectively. Altogether, both EDGAR versions exhibit a significant underestimation of agricultural emissions. Seasonal differences are likely one cause for the large difference in correction factors between 2017 and 2019. Additionally, during the 2019 aircraft campaign, an extreme flooding event occurred that likely influenced our results (discussed below). Although EDGAR4.3.2 exhibits a seasonal cycle, its agricultural correction factor also varies considerably between 2017 and 2019. Hence, the seasonality is not captured in the EDGAR inventory for the Midwest, which appears to be caused by the flooding. Figure 3c displays the EDGAR5.0 average Midwest emissions for each flight day with non-optimized and optimized agricultural emissions. For EDGAR4.3.2 the optimized result is (nearly) the same as both versions differ (nearly) only in their strength of E_{AGR} which is adjusted in the course of the optimization. On average, optimized total N_2O emissions are $0.42 \pm 0.28\,\mathrm{nmol\,m^{-2}\,s^{-1}}$ in 2017 and $1.06 \pm 0.57\,\mathrm{nmol\,m^{-2}\,s^{-1}}$ in 2019.

Optimized emissions for June/July 2019 are 2–3 times higher compared to DayCent emissions. Despite this, DayCent emissions are closer to our optimized emissions compared to EDGAR during the same period. In contrast, DayCent and EDGAR emissions are both too low by a similar magnitude in October compared to our optimized results. Hence, as DayCent considers regional characteristics, it performs much better on the regional scale in the summer than the emission factor approach that is used in the EDGAR inventory. A more quantitative evaluation of DayCent would require surface flux calculations for 2017 and 2019 incorporating the corresponding regional conditions like weather, soil conditions, and N-fertilizer application rate and time. DayCent has not been applied to estimate emissions specific to 2017 and 2019 so it is not clear if the model would underestimate the values for these years although this may be the case given the historical data from 2011–2015.

Fu et al. (2017) reported emissions of 3.00–$4.38\,\mathrm{nmol\,m^{-2}\,s^{-1}}$ during June 1-20, 2010 for the Corn Belt, which is significantly higher than our estimates for June/July 2019. Griffis et al. (2013) estimated the Corn Belt emissions to be around $2\,\mathrm{nmol\,m^{-2}\,s^{-1}}$ and $1\,\mathrm{nmol\,m^{-2}\,s^{-1}}$ in June/July 2010 and 2011, respectively, which is consistent with our findings. Kort et al. (2008) and Miller et al. (2012) derived scaling factors for the central U.S. To be able to compare their results to ours, we estimated the corresponding flux densities for the Midwest region using their scaling factors for the respective EDGAR versions. Kort et al. (2008) derived $0.54\,\mathrm{nmol\,m^{-2}\,s^{-1}}$ for May/June 2003 and Miller et al. (2012) $0.57/0.25\,\mathrm{nmol\,m^{-2}\,s^{-1}}$ and $0.94/0.53\,\mathrm{nmol\,m^{-2}\,s^{-1}}$ for June/July 2004 and 2008, respectively. Both studies show lower values than our estimate. Miller et al. (2012) stated that maximum emissions occurred in June. Our DayCent calculations are also highest in June. This could partly explain our lower estimates compared to Fu et al. (2017) as we report for the end of June/beginning of July after the expected emission peak. Moreover, Fu et al. (2017) only scaled Corn Belt emissions and kept other regions unmodified which could lead to higher estimates, if they sampled other regions with lower emission rates than the Corn Belt. Overall, our estimates are in the range of previous top-down studies. However, the spread among the studies is large.

The nature of soil N_2O emissions leads to significant temporal variability in the emissions that is not represented in the EDGAR inventory. Unlike EDGAR, DayCent is capable of representing those variations to a certain extent. In our 2011–2015 calculations the monthly standard deviations range from 10 % in October to 21 % in July, demonstrating the strong interannual variability. Furthermore, weather conditions in the study domain in 2019 were unusually extreme. During the campaign, the U.S. was experiencing its wettest period in 125 years, with severe flooding in the Midwest (NOAA, 2020) forcing the farmers to significantly delay planting in the affected regions (USDA, 2020) and postponing the peak emission period. Depending on whether the zenith is shifted closer to or further away from our investigated period in June/July this event may have either amplified or lowered our emission estimates. Additionally, the above-average humidity might have enhanced soil N_2O emissions leading to higher estimates (Butterbach-Bahl et al., 2013). The influence of this flooding event cannot be quantified within this study, as this would require more data over longer periods spanning the whole event. However, in a follow-up study we plan to use DayCent simulations driven with those flooding conditions to gain insights on how soil N_2O emissions were affected.

4 Conclusion

Unique continuous in situ airborne N_2O measurements of ten research flights were used to quantify N_2O emissions in the U.S. Midwest using a top-down approach. In October 2017 and June/July 2019 agricultural Midwest emission were on average $6.3 \pm 4.6/3.5 \pm 2.7$ and $11.4 \pm 6.6/9.9 \pm 5.7$ times higher than EDGAR4.3.2/EDGAR5.0 estimates resulting in $0.42 \pm 0.28\,\mathrm{nmol\,m^{-2}\,s^{-1}}$ and $1.06 \pm 0.57\,\mathrm{nmol\,m^{-2}\,s^{-1}}$ Midwest emissions, respectively. Our 2019 estimates were most likely influenced by an extreme flooding event, which is difficult to capture in EDGAR as the inventory uses a more climatological average emissions dataset. Agricultural soil emissions estimated with DayCent in 2011–2015 were 0.32–0.48, 0.16–0.30, and 0.08–0.11 $\mathrm{nmol\,m^{-2}\,s^{-1}}$ in June, July, and October, respectively. Based on these historical emission estimates, this is higher than non-optimized EDGAR emissions, but still significantly lower than our optimized fluxes. Our findings are in the range of previous top-down estimates for the Corn Belt and central U.S. However, a quantitative comparison of those studies show that the range of derived N_2O surface fluxes is large, likely due to the temporal complexity of N_2O soil emissions.

More N_2O focused studies are necessary to fully understand the drivers of Midwest N_2O emissions and the most appropriate modeling methods to estimate emission patterns. To cover the high temporal variability on various scales, long term projects with regular airborne measurements spanning wide areas of the Midwest are necessary. Combining a process-based model like DayCent capable of simulating the temporal and spatial variability of N_2O emissions, with extensive airborne and tall tower top-down studies at selected spots and times, could be a cost effective approach that would limit the number of flights needed to produce accurate estimates for the region and improve national reporting of emissions (Ogle et al., 2020). As interest grows in expanding efforts to reduce N_2O emissions (Kanter et al., 2020), improved quantification of N_2O surface fluxes is mandatory for policy makers to be able to develop effective mitigation strategies.

Acknowledgments
The ACT-America project is a NASA Earth Venture Suborbital-2 project funded by NASA's Earth Science Division (grant NNX15AG76G to the Pennsylvania State University). All ACT-America flask and in situ data used in this manuscript can be found online (at `https://daac.ornl.gov/cgi-bin/dataset_lister.pl?p=37`). We thank DLR VO-R for funding the young investigator research group "Greenhouse Gases".

References

Baier, B. C., Sweeney, C., Choi, Y., Davis, K. J., DiGangi, J. P., Feng, S., ... Weibring, P. (2020). Multispecies Assessment of Factors Influencing Regional CO_2 and CH_4 Enhancements During the Winter 2017 ACT-America Campaign. *Journal of Geophysical Research: Atmospheres*, *125*, e2019JD031339. doi: 10.1029/2019JD031339

Barkley, Z. R., Davis, K. J., Feng, S., Balashov, N., Fried, A., DiGangi, J., ... Halliday, H. S. (2019). Forward Modeling and Optimization of Methane Emissions in the South Central United States Using Aircraft Transects Across Frontal Boundaries. *Geophysical Research Letters*, *46*(22), 13564–13573. doi: 10.1029/2019gl084495

Barkley, Z. R., Lauvaux, T., Davis, K. J., Deng, A., Fried, A., Weibring, P., ... Dickerson, R. R. (2019). Estimating Methane Emissions From Underground Coal and Natural Gas Production in Southwestern Pennsylvania. *Geophysical Research Letters*, *46*(8), 4531–4540. doi: 10.1029/2019GL082131

Barkley, Z. R., Lauvaux, T., Davis, K. J., Deng, A., Miles, N. L., Richardson, S. J., ... Maasakkers, J. D. (2017). Quantifying methane emissions from natural gas production in north-eastern Pennsylvania. *Atmospheric Chemistry and Physics*, *17*(22), 13941–13966. doi: 10.5194/acp-17-13941-2017

Butterbach-Bahl, K., Baggs, E. M., Dannenmann, M., Kiese, R., & Zechmeister-Boltenstern, S. (2013). Nitrous oxide emissions from soils: how well do we understand the processes and their controls? *Philosophical Transactions of the Royal Society B: Biological Sciences*, *368*, 20130122. doi: 10.1098/rstb.2013.0122

Chen, Z., Griffis, T. J., Millet, D. B., Wood, J. D., Lee, X., Baker, J. M., ... Wells, K. C. (2016). Partitioning N_2O emissions within the U.S. Corn Belt using an inverse modeling approach. *Global Biogeochemical Cycles*, *30*(8), 1192–1205. doi: 10.1002/2015gb005313

Ciais, P., Sabine, C., Bala, G., Bopp, L., Brovkin, V., Canadell, J., ... Thornton, P. (2013). Carbon and Other Biogeochemical Cycles. In T. F. Stocker et al. (Eds.), *Climate Change 2013: The Physical Science Basis. Contribution of Working Group I to the Fifth Assessment Report of the Intergovernmental Panel on Climate Change* (pp. 465–570). Cambridge, United Kingdom and New York, NY, USA: Cambridge University Press.

Crippa, M., Solazzo, E., Huang, G., Guizzardi, D., Koffi, E., Muntean, M., ... Janssens-Maenhout, G. (2020). High resolution temporal profiles in the Emissions Database for Global Atmospheric Research. *Scientific Data*, *7*(121). doi: 10.1038/s41597-020-0462-2

Del Grosso, S. J., Parton, W. J., Keough, C. A., & Reyes-Fox, M. (2011). Special features of the DayCent modeling package and additional procedures for parameterization, calibration, validation, and applications. In L. R. Ahuja & L. Ma (Eds.), *Methods of Introducing System Models into Agricultural Research* (pp. 155–176). Madison, WI, USA: American Society of Agronomy, Crop Science Society of America, Soil Science Society of America. doi: 10.2134/advagricsystmodel2.c5

Del Grosso, S. J., Parton, W. J., Mosier, A. R., Hartman, M. D., Brenner, J., Ojima, D. S., & Schimel, D. S. (2001). Simulated Interaction of Carbon Dynamics and Nitrogen Trace Gas Fluxes Using the DAYCENT Model. In M. Schaffer, L. Ma, & S. Hansen (Eds.), *Modeling Carbon and Nitrogen Dynamics for Soil Management* (pp. 303–332). Boca Raton, Florida, USA: CRC Press.

Díaz-Isaac, L. I., Lauvaux, T., & Davis, K. J. (2018). Impact of physical parameterizations and initial conditions on simulated atmospheric transport and CO_2 mole fractions in the US Midwest. *Atmospheric Chemistry and Physics*, *18*(20), 14813–14835. doi: 10.5194/acp-18-14813-2018

EDGAR. (2020). *Emission Database for Global Atmospheric Research.* Retrieved from `https://edgar.jrc.ec.europa.eu/` (last accessed: 20 Jul 2020)

EDGAR4.3.2. (2017). *Emissions Database for Global Atmospheric Research, version 4.3.2.* European Comission. Retrieved from `https://edgar.jrc.ec.europa.eu/overview.php?v=432_GHG` doi: https://data.europa.eu/doi/10.2904/JRC-DATASET-EDGAR

EDGAR5.0. (2019). *Emissions Database for Global Atmospheric Research, version 5.0.* European Comission. Retrieved from `https://edgar.jrc.ec.europa.eu/overview.php?v=50_GHG` doi: https://data.europa.eu/doi/10.2904/JRC-DATASET-EDGAR

EPA. (2020). *Inventory of U.S. Greenhouse Gas Emissions and Sinks: 1990–2018.* United States Environmental Protection Agency. EPA 430-R-20-002. Retrieved from `https://www.epa.gov/ghgemissions/inventory-us-greenhouse-gas-emissions-and-sinks-1990-2018`

ERA5. (2017). *Copernicus Climate Change Service (C3S) (2017): ERA5: Fifth generation of ECMWF atmospheric reanalyses of the global climate.* Copernicus Climate Change Service Climate Data Store (CDS). Retrieved from `https://cds.climate.copernicus.eu/cdsapp#!/home` (last accessed: 02 Mar 2020)

FAO. (2020). *Food and Agriculture Organization of the United Nations - FAOSTAT.* Retrieved from `http://www.fao.org/faostat/en/#compare` (last accessed: 20 Jul 2020)

Fu, C., Lee, X., Griffis, T. J., Dlugokencky, E. J., & Andrews, A. E. (2017). Investigation of the N_2O emission strength in the U. S. Corn Belt. *Atmospheric Research*, *194*, 66–77. doi: 10.1016/j.atmosres.2017.04.027

GDAS-FNL. (2015). *National Centers for Environmental Prediction, National Weather Service, NOAA, U.S. Department of Commerce: NCEP GDAS/FNL 0.25 Degree Global Tropospheric Analyses and Forecast Grids, updated daily.* Research Data Archive at the National Center for Atmospheric Research, Computational and Information Systems Laboratory. (last accessed: 28 May 2020) doi: 10.5065/D65Q4T4Z

Grell, G. A., Peckham, S. E., Schmitz, R., McKeen, S. A., Frost, G., Skamarock, W. C., & Eder, B. (2005). Fully coupled "online" chemistry within the WRF model. *Atmospheric Environment*, *39*(37), 6957–6975. doi: 10.1016/j.atmosenv.2005.04.027

Griffis, T. J., Lee, X., Baker, J. M., Russelle, M. P., Zhang, X., Venterea, R., & Millet, D. B. (2013). Reconciling the differences between top-down and bottom-up estimates of nitrous oxide emissions for the U.S. Corn Belt. *Global Biogeochemical Cycles*, *27*(3), 746–754. doi: 10.1002/gbc.20066

Hall, B. D., Dutton, G. S., & Elkins, J. W. (2007). The NOAA nitrous oxide standard scale for atmospheric observations. *Journal of Geophysical Research: Atmospheres*, *112*, D09305. doi: 10.1029/2006JD007954

Hersbach, H., Bell, B., Berrisford, P., Hirahara, S., Horányi, A., Muñoz Sabater, J., ... Thépaut, J.-N. (2020). The ERA5 global reanalysis. *Quarterly Journal of the Royal Meteorological Society*, 1–51. doi: 10.1002/qj.3803

Janssens-Maenhout, G., Crippa, M., Guizzardi, D., Muntean, M., Schaaf, E., Dentener, F., ... Oreggioni, G. D. (2019). EDGAR v4.3.2 Global Atlas of the three major greenhouse gas emissions for the period 1970–2012. *Earth System Science Data*, *11*(3), 959–1002. doi: 10.5194/essd-11-959-2019

Kanter, D. R., Ogle, S. M., & Winiwarter, W. (2020). Building on Paris: integrating nitrous oxide mitigation into future climate policy. *Current Opinion in Environmental Sustainability*, *47*, 1–6. doi: 10.1016/j.cosust.2020.04.005

Kort, E. A., Eluszkiewicz, J., Stephens, B. B., Miller, J. B., Gerbig, C., Nehrkorn, T., ... Wofsy, S. C. (2008). Emissions of CH_4 and N_2O over the United States and Canada based on a receptor-oriented modeling framework and COBRA-NA atmospheric observations. *Geophysical Research Letters*, *35*, L18808. doi: 10.1029/2008GL034031

Kostinek, J., Roiger, A., Davis, K. J., Sweeney, C., DiGangi, J. P., Choi, Y., ... Butz, A. (2019). Adaptation and performance assessment of a quantum and interband cascade laser spectrometer for simultaneous airborne in situ observation of CH_4, C_2H_6, CO_2, CO and N_2O. *Atmospheric Measurement Techniques*, *12*(3), 1767–1783. doi: 10.5194/amt-12-1767-2019

MacFarling Meure, C., Etheridge, D., Trudinger, C., Steele, P., Langenfelds, R., van Ommen, T., ... Elkins, J. (2006). Law Dome CO_2, CH_4 and N_2O ice core records extended to 2000 years BP. *Geophysical Research Letters*, *33*(14). doi: 10.1029/2006GL026152

Miller, S. M., Kort, E. A., Hirsch, A. I., Dlugokencky, E. J., Andrews, A. E., Xu, X., ... Wofsy, S. C. (2012). Regional sources of nitrous oxide over the United States: Seasonal variation and spatial distribution. *Journal of Geophysical Research: Atmospheres*, *117*, D06310. doi: 10.1029/2011JD016951

Myhre, G., Shindell, D., Bréon, F.-M., Collins, W., Fuglestvedt, J., Huang, J., ... Zhang, H. (2013). Anthropogenic and Natural Radiative Forcing. In T. F. Stocker et al. (Eds.), *Climate Change 2013: The Physical Science Basis. Contribution of Working Group I to the Fifth Assessment Report of the Intergovernmental Panel on Climate Change* (pp. 659–740). Cambridge, United Kingdom and New York, NY, USA: Cambridge University Press.

NARR. (2005). *National Centers for Environmental Prediction, National Weather Service, NOAA, U.S. Department of Commerce: NCEP North American Regional Reanalysis, updated monthly.* Research Data Archive at the National Center for Atmospheric Research, Computational and Information Systems Laboratory. Retrieved from https://rda.ucar.edu/datasets/ds608.0 (last accessed: 27 May 2020)

NOAA. (2020). *National Centers for Environmental Information: Climate at a Glance - Rankings.* Retrieved from https://www.ncdc.noaa.gov/cag/ (last accessed: 20 Jul 2020)

NOAA-ESRL. (2020). *Combined Nitrous Oxide data from the NOAA/ESRL Global Monitoring Division.* Retrieved from https://www.esrl.noaa.gov/gmd/hats/combined/N2O.html (last accessed: 20 Jul 2020)

NOAA-NCEI. (2020). *U.S. Billion-Dollar Weather and Climate Disasters.* NOAA National Centers for Environmental Information (NCEI). Retrieved from https://www.ncdc.noaa.gov/billions/ doi: 10.25921/stkw-7w73

Ogle, S. M., Butterbach-Bahl, K., Cardenas, L., Skiba, U., & Scheer, C. (2020). From research to policy: optimizing the design of a national monitoring system to mitigate soil nitrous oxide emissions. *Current Opinion in Environmental Sustainability*, *47*, 28–36. doi: 10.1016/j.cosust.2020.06.003

Olivier, J. G. J., Bouwman, A. F., Berdowski, J. J. M., Veldt, C., Bloos, J. P. J., Visschedijk, A. J. H., ... Zandveld, P. Y. J. (1999). Sectoral emission inventories of greenhouse gases for 1990 on a per country basis as well as on 1°×1°. *Environmental Science & Policy*, *2*(3), 241–263. doi: 10.1016/s1462-9011(99)00027-1

Olivier, J. G. J., Bouwman, A. F., van der Maas, C. W. M., Berdowski, J. J. M., Veldt, C., Bloos, J. P. J., ... Haverlag, J. L. (1996). Description of EDGAR Version 2.0: A set of global emission inventories of greenhouse gases and ozone-depleting substances for all anthropogenic and most natural sources on a per country basis and on 1°×1° grid. *National Institute of Public Health and the Environment (RIVM) report no. 771060 002 / TNO-MEP report no. R96/119*. Retrieved from http://hdl.handle.net/10029/10497

Park, S., Croteau, P., Boering, K. A., Etheridge, D. M., Ferretti, D., Fraser, P. J., ... M., T. C. (2012). Trends and seasonal cycles in the isotopic composition of nitrous oxide since 1940. *Nature Geoscience*, *5*(4), 261–265. doi: 10.1038/ngeo1421

Parton, W. J., Hartman, M., Ojima, D., & Schimel, D. (1998). DAYCENT and its land surface submodel: description and testing. *Global and Planetary Change*, *19*(1), 35–48. doi: 10.1016/S0921-8181(98)00040-X

Paustian, K., Lehmann, J., Ogle, S. M., Reay, D., Robertson, G. P., & Smith, P. (2016). Climate-smart soils. *Nature*, *532*, 49–57. doi: 10.1038/nature17174

Prather, M. J., Hsu, J., DeLuca, N. M., Jackman, C. H., Oman, L. D., Douglass, A. R., ... Funke, B. (2015). Measuring and modeling the lifetime of nitrous oxide including its variability. *Journal of Geophysical Research: Atmospheres*, *120*(11), 5693–5705. doi: 10.1002/2015jd023267

Ravishankara, A. R., Daniel, J. S., & Portmann, R. W. (2009). Nitrous Oxide (N_2O): The Dominant Ozone-Depleting Substance Emitted in the 21st Century. *Science*, *326*(5949), 123–125. doi: 10.1126/science.1176985

Reay, D. S., Davidson, E. A., Smith, K. A., Smith, P., Melillo, J. M., Dentener, F., & Crutzen, P. J. (2012). Global agriculture and nitrous oxide emissions. *Nature Climate Change*, *2*(6), 410–416. doi: 10.1038/nclimate1458

Stehfest, E., & Bouwman, L. (2006). N_2O and NO emission from agricultural fields and soils under natural vegetation: summarizing available measurement data and modeling of global annual emissions. *Nutrient Cycling in Agroecosystems*, *74*(3), 207–228. doi: 10.1007/s10705-006-9000-7

Sweeney, C., Baier, B. C., Miller, J. B., Lang, P., Miller, B. R., Lehman, S., ... Yang, M. M. (2018). *ACT-America: L2 In Situ Atmospheric Gas Concentrations from Flasks, Eastern USA.* ORNL Distributed Active Archive Center. Retrieved from `https://daac.ornl.gov/cgi-bin/dsviewer.pl?ds_id=1575` doi: 10.3334/ORNLDAAC/1575

Sweeney, C., Karion, A., Wolter, S., Newberger, T., Guenther, D., Higgs, J. A., ... Tans, P. P. (2015). Seasonal climatology of CO_2 across North America from aircraft measurements in the NOAA/ESRL Global Greenhouse Gas Reference Network. *Journal of Geophysical Research: Atmospheres*, *120*(10), 5155–5190. doi: 10.1002/2014jd022591

Thompson, R. L., Lassaletta, L., Patra, P. K., Wilson, C., Wells, K. C., Gressent, A., ... Canadell, J. G. (2019). Acceleration of global N_2O emissions seen from two decades of atmospheric inversion. *Nature Climate Change*, *9*(12), 993–998. doi: 10.1038/s41558-019-0613-7

Tian, H., Xu, R., Canadell, J. G., Thompson, R. L., Winiwarter, W., Suntharalingam, P., ... Yao, Y. (2020). A comprehensive quantification of global nitrous oxide sources and sinks. *Nature*, *586*, 248–256. doi: 10.1038/s41586-020-2780-0

USDA. (2020). *Economics, Statistics and Market Information System - Crop Progress.* Retrieved from `https://usda.library.cornell.edu/concern/publications/8336h188j?locale=en#release-items` (last accessed: 20 Jul 2020)

USDA-NASS. (2020). *United States Department of Agriculture - National Agricultural Statistics Service - Statistics by State.* Retrieved from `https://www.nass.usda.gov/Statistics_by_State/index.php` (last accessed: 23 Jul 2020)

Supporting Information for "Quantifying nitrous oxide emissions in the U.S. Midwest - A top-down study using high resolution airborne in-situ observations"

Maximilian Eckl[1], Anke Roiger[1], Julian Kostinek[1], Alina Fiehn[1], Heidi Huntrieser[1], Christoph Knote[2], Zachary R. Barkley[3], Stephen M. Ogle[4], Bianca C. Baier [5,6], Colm Sweeney[6], and Kenneth J. Davis[3,7]

[1]Deutsches Zentrum für Luft- und Raumfahrt (DLR), Institut für Physik der Atmosphäre, Oberpfaffenhofen, Germany

[2]Ludwig-Maximilians-University (LMU), Meteorological Institute, Munich, Germany

[3]Department of Meteorology and Atmospheric Science, Pennsylvania State University, University Park, PA, USA

[4]Natural Resource Ecology Laboratory, Colorado State University, Fort Collins, CO, USA

[5]Cooperative Institute for Research in Environmental Sciences, University of Colorado-Boulder, Boulder, CO, USA

[6]NOAA Global Monitoring Laboratory, Boulder, CO, USA

[7]Earth and Environmental Systems Institute, Pennsylvania State University, University Park, PA, USA

Corresponding author: M. Eckl, Institut für Physik der Atmosphäre, Deutsches Zentrum für Luft- und Raumfahrt (DLR), Münchener Straße 20, 82234 Weßling, Germany. (Maximilian.Eckl@dlr.de)

Contents of this file

Introduction

Here we provide additional information on the employed model setup (Text S1), the EDGAR sectors (Text S2 and Table S1), the linear relationship between the tracer integral along a transect and the emission strength (Text S3 and Table S2), the uncertainties in the Monte Carlo simulations (Text S4), the influence of the bias correction on the results (Text S5 and Table S3), the background (Figure S1), and the model performance (Figure S2 and S3).

Text S1: Model setup

Simulations are performed with WRF-Chem version 4.0.2. The employed model physics configuration includes the Thompson scheme for microphysics, RRTMG for radiation, Kain-Fritsch for cumulus parameterization, MYNN 2.5 level TKE for PBL physics and the Noah land-surface model. Vertically, each domain encompasses 50 terrain-following layers, with a greater resolution near the ground. Two-way nesting enables information transfer between the domains. Moreover, we use the WRF Four Dimensional Data Assimilation (FDDA) feature to perform analysis nudging in the outer domain, to ensure an optimal meteorological model solution.

Text S2: EDGAR sector description

We merge the different EDGAR sectors into three main sectors: Agricultural E_{AGR}, non-agricultural anthropogenic E_{nonAGR}, and natural emissions E_N. E_{AGR} covers emissions from agricultural soils, indirect emissions from agricultural soils, manure management, and agricultural waste burning, whereas E_{nonAGR} consists of all remaining anthropogenic EDGAR sectors, including (among others) road transportation, chemical processes, and power industry. E_N encompasses natural soil and ocean emissions. As emissions from oceans did not contribute to Midwest N_2O enhancements in our simulations, our E_N involves only natural soil emissions. The applied assumption that all those sources originate from the surface is valid except for aviation related emissions. Since those account for less than 0.3 % of the yearly total EDGAR Midwest emissions, we excluded them from E_{nonAGR} under the assumption that this would not have a significant impact on our results. A detailed listing of all EDGAR sectors can be found in Table S1.

Text S3: Linearity of tracer integral and emission strength

For each flight the area summed agricultural emissions E_{AGR}^{sum} are linear to the corresponding tracer integral along a transect A_{AGR}. This implies that if agricultural emissions are scaled by a certain factor, the tracer integral is also scaled by this factor. To verify this, we simulated each flight day with a E_{AGR} multiplied by 10, 20, and 30 (F_{AGR}^{E}) and compared those factors with the resulting magnitude of enlargement in A_{AGR} (F_{AGR}^{A}). A linear regression between F_{AGR}^{E} and F_{AGR}^{A} (see Table S2) exhibits negligible residuals and a slope and y-intercept which differs insignificantly from one and zero, respectively, proving the equivalence of F_{AGR}^{E} and F_{AGR}^{A}.

Text S4: Uncertainties in Monte Carlo simulation

The uncertainties of the observed background ($\sigma = \pm 0.5$ ppb and $\sigma = \pm 0.9$ ppb for 2017 and 2019, respectively) are the standard deviation of all 2^{nd} low level leg percentiles of a whole campaign. The background uncertainties are dominated by large scale circulations and long term variability such as seasons, and are probably not normally distributed. However, too few observations prevent the determination of the actual distribution. Here, we assume that a normal distribution is the best first order guess. Janssens-Maenhout et al. (2019) states the relative $1\,\sigma$ uncertainty of total EDGAR4.3.2 N_2O emissions in the U.S. to be 21 %. No sector-specific uncertainty is provided. Hence, we use this value as a rough estimate for the uncertainty of only non agricultural emissions. As we could not find uncertainty estimates for EDGAR5.0 and EDGAR2 we assume them to be the same and twice as in EDGAR4.3.2, respectively. For days with large agricultural correction factors F_{AGR} the uncertainties of E_{nonAGR} and E_N affect the results only marginally. Hence, this uncertainty analysis is implicitly based on the assumption that E_{nonAGR} and E_N are well represented in the inventories compared to E_{AGR}. Following Butterbach-Bahl, Baggs, Dannenmann, Kiese, and Zechmeister-Boltenstern (2013) mainly N_2O emissions from soils account for the uncertainty in N_2O budgets on regional and national scales, which supports our assumption.

Text S5: Bias correction

Following Barkley et al. (2019), the bias due to an erroneous modeled wind speed and PBL height can be corrected with:

$$C_{mod}^{corr} = C_{mod} \cdot \frac{U_{mod} \cdot Z_{mod}}{U_{obs} \cdot Z_{obs}} \tag{1}$$

Here, C_{mod} is the modeled N_2O enhancement along a transect and C_{mod}^{corr} the corresponding bias corrected one, which is further used for the model optimization. U_{mod}/U_{obs} is the modeled/observed wind speed averaged along the transect. For the observed PBL height Z_{obs} we use in situ soundings conducted with the C-130 at the beginning, the end, and during the transect. For each flown sounding the PBL height is determined as the lowest (regarding altitude) significant maximum of the observed virtual potential temperature lapse rate profile. The average of all determined PBL heights defines Z_{obs} of the transect. For the modeled PBL height of a transect Z_{mod} we use the modeled profiles at the grid points closest to the flown soundings and perform the same approach as for Z_{obs}. However, there is a caveat here. We correct for model errors at the position of the aircraft at a certain time but we are simulating large areas for several days. The model error varies over space and time, thus, limiting the benefit of the posed bias correction. Table S3 summarizes the results of the bias correction.

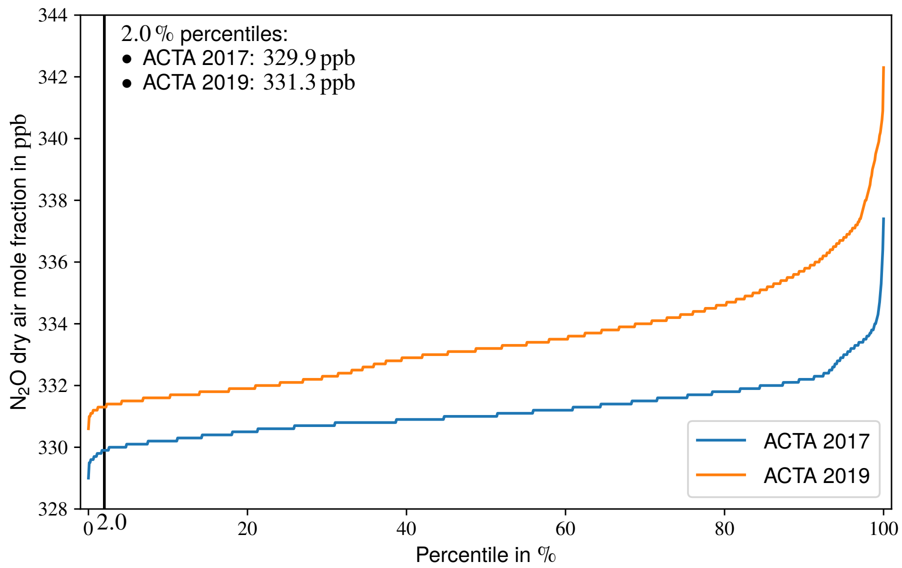

Figure S1. Percentiles for ACTA 2017 and ACTA 2019. Low level legs (at approx. 1000 ft AGL) of all conducted flights were merged and the corresponding percentiles were calculated.

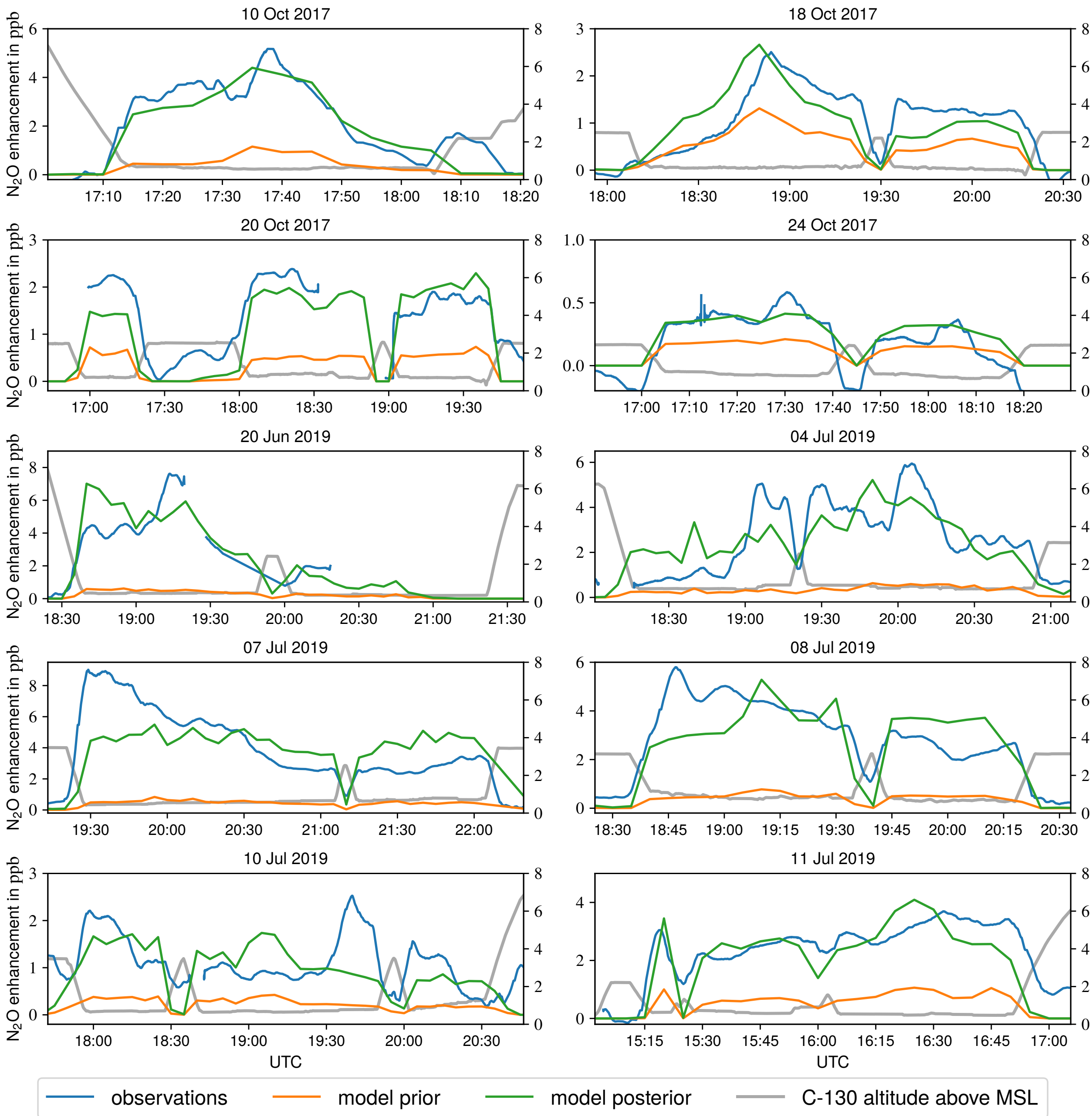

Figure S2. Observed vs. modeled N_2O enhancement (emitted from EDGAR4.3.2/EDGAR2 $E_{AGR} + E_{nonAGR} + E_N$) for each of the ten investigated flights. For an easier visual comparison the 5 min-moving average of the observations is shown. The modeled enhancements are the mean from the three model runs with different initial and boundary meteorological conditions (ERA5, GDAS-FNL, and NARR) on the closest grid points in space and time to each observation.

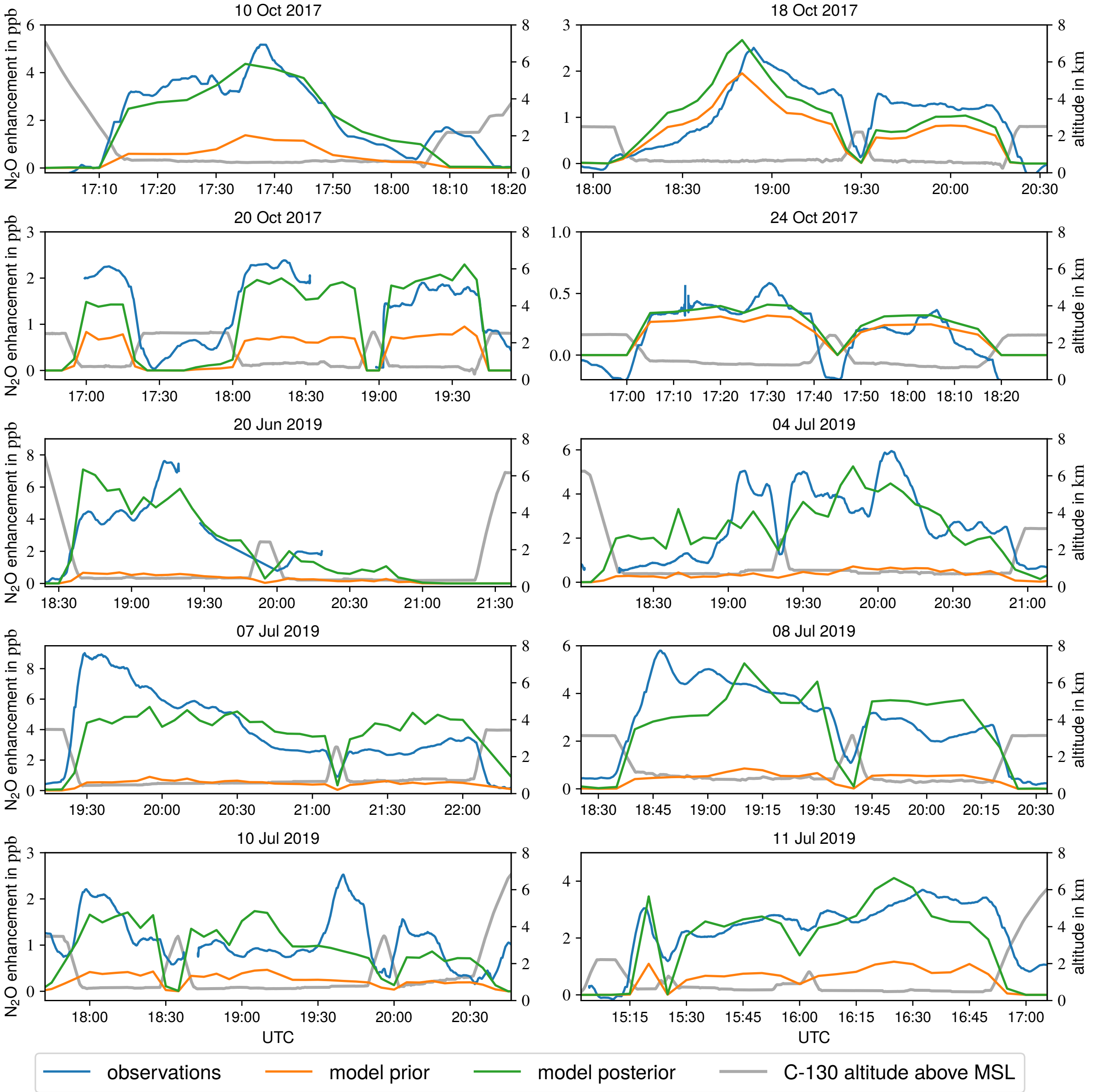

Figure S3. As Figure S2 but modeled N_2O enhancement emitted from EDGAR5.0/EDGAR2 $E_{AGR} + E_{nonAGR} + E_N$.

Table S1. Components of E_{AGR}, E_{nonAGR}, and E_N. If not otherwise specified, sectors are included in EDGAR4.3.2 and EDGAR5.0. All existing EDGAR4.3.2/EDGAR5.0 N_2O sectors are listed as well as all natural EDGAR2 sectors.

main sector	EDGAR sector	IPCC (2006b) code
E_{AGR}	Manure management	3A2
	Agricultural waste burning	3C1b
	Agricultural soils	3C2+3C3+3C4+3C7
	Indirect N_2O emissions from agriculture	3C5+3C6
E_{nonAGR}	Power industry	1A1a
	Oil refineries and transformation industry	1A1b+1A1ci+1A1cii+1A5biii+1B1b+ 1B2aiii6+1B2biii3+1B1c
	Combustion for manufacturing	1A2
	Road transportation	1A3b
	Railways, pipelines, off-road transport	1A3c+1A3e
	Shipping	1A3d
	Energy for buildings	1A4+1A5
	Fuel exploitation	1B1a+1B2aiii2+1B2aiii3+1B2bi+ 1B2bii
	Chemical processes	2B
	Solvents and products use	2D3+2E+2F+2G
	Solid waste landfills	4A+4B
	Solid waste incineration	4C
	Waste water handling	4D
	Indirect emissions from NO_x and NH_3	5A
	Fossil fuel fires	5B
E_N	Natural soils (just EDGAR2)	–
excluded	Aviation climbing and descent	1A3a_CDS
	Aviation cruise	1A3a_CRS
	Aviation landing and takeoff	1A3a_LTO
	Aviation supersonic	1A3a_SPS
	Oceans (just EDGAR2)	–

Table S2. Results of a linear regression between F^E_{AGR} and F^A_{AGR} and their correlation R. Every flight day was simulated with a F^E_{AGR} of 10, 20, and 30 and the corresponding F^A_{AGR} was calculated. The regression was performed via a least squares polynomial fit. The residual is the squared Euclidean 2-norm. See Text S3 for a description of F^E_{AGR} and F^A_{AGR}.

EDGAR version	slope	slope−1	y-intercept	residual	R	R-1
v4.3.2	1.0	-0.05×10^{-3}	-0.47×10^{-3}	0.02×10^{-3}	1.0	-0.02×10^{-7}
v5.0	1.0	1.28×10^{-3}	-1.26×10^{-3}	3.39×10^{-3}	1.0	-3.6×10^{-7}

Table S3. Modeled vs. observed wind speed and PBL height for each flight and the corresponding bias correction factor. In the model columns the first value belongs to the ERA5, the second to the GDAS-FNL, and the third to the NARR simulation.

Day	U_{obs} in m s^{-1}	U_{mod} in m s^{-1}	$\frac{U_{mod}}{U_{obs}}$	Z_{obs} in m	Z_{mod} in m	$\frac{Z_{obs}}{Z_{mod}}$	$\frac{U_{mod} \cdot Z_{mod}}{U_{obs} \cdot Z_{obs}}$
		5.2	1.5		1134	1.1	1.6
10 Oct 2017	3.5	3.0	0.9	1067	1319	1.2	1.1
		3.7	1.1		1325	1.2	1.3
		12.9	1.2		1106	0.8	0.9
18 Oct 2017	10.6	12.9	1.2	1417	1307	0.9	1.1
		12.8	1.2		1116	0.8	1.0
		17.9	1.4		963	0.8	1.0
20 Oct 2017	13.1	17.3	1.3	1273	1013	0.8	1.1
		17.2	1.3		1084	0.9	1.1
		15.9	1.0		1565	1.0	1.0
24 Oct 2017	15.7	15.9	1.0	1603	1716	1.1	1.1
		15.5	1.0		1668	1.0	1.0
		9.1	1.3		1024	0.7	0.9
20 Jun 2019	7.1	9.0	1.3	1480	1188	0.8	1.0
		8.4	1.2		1094	0.7	0.9
		5.1	1.0		1784	1.1	1.1
04 Jul 2019	4.9	4.3	0.9	1684	1944	1.2	1.0
		3.5	0.7		2080	1.2	0.9
		4.6	1.1		2417	1.3	1.4
07 Jul 2019	4.3	3.7	0.9	1889	2420	1.3	1.1
		3.5	0.8		2246	1.2	1.0
		10.2	1.1		1955	1.1	1.3
08 Jul 2019	9.0	10.1	1.1	1718	2055	1.2	1.3
		9.3	1.0		1994	1.2	1.2
		10.2	1.0		1956	1.1	1.1
10 Jul 2019	10.4	10.9	1.0	1767	1893	1.1	1.1
		10.2	1.0		2014	1.1	1.1
		7.3	1.1		1861	1.1	1.2
11 Jul 2019	6.7	5.8	0.9	1659	1638	1.0	0.9
		6.6	1.0		1608	1.0	1.0

References

Barkley, Z. R., Davis, K. J., Feng, S., Balashov, N., Fried, A., DiGangi, J., ... Halliday, H. S. (2019). Forward Modeling and Optimization of Methane Emissions in the South Central United States Using Aircraft Transects Across Frontal Boundaries. *Geophysical Research Letters*, *46*(22), 13564–13573. doi: 10.1029/2019gl084495

Butterbach-Bahl, K., Baggs, E. M., Dannenmann, M., Kiese, R., & Zechmeister-Boltenstern, S. (2013). Nitrous oxide emissions from soils: how well do we understand the processes and their controls? *Philosophical Transactions of the Royal Society B: Biological Sciences*, *368*, 20130122. doi: 10.1098/rstb.2013.0122

Janssens-Maenhout, G., Crippa, M., Guizzardi, D., Muntean, M., Schaaf, E., Dentener, F., ... Oreggioni, G. D. (2019). EDGAR v4.3.2 Global Atlas of the three major greenhouse gas emissions for the period 1970–2012. *Earth System Science Data*, *11*(3), 959–1002. doi: 10.5194/essd-11-959-2019